

Journal of Materials Chemistry B

Materials for biology and medicine

Accepted Manuscript

This article can be cited before page numbers have been issued, to do this please use: D. Carta, C. CAVAZZOLI, R. D. Pasquale, Z. MOghaddam, H. Zhao, A. Hoxha, L. Lewendon, M. Felipe-Sotelo, C. Crean, A. Zambon, G. Lusvardi and J. Merino Gutierrez, *J. Mater. Chem. B*, 2025, DOI: 10.1039/D5TB00454C.



This is an Accepted Manuscript, which has been through the Royal Society of Chemistry peer review process and has been accepted for publication.

Accepted Manuscripts are published online shortly after acceptance, before technical editing, formatting and proof reading. Using this free service, authors can make their results available to the community, in citable form, before we publish the edited article. We will replace this Accepted Manuscript with the edited and formatted Advance Article as soon as it is available.

You can find more information about Accepted Manuscripts in the [Information for Authors](#).

Please note that technical editing may introduce minor changes to the text and/or graphics, which may alter content. The journal's standard [Terms & Conditions](#) and the [Ethical guidelines](#) still apply. In no event shall the Royal Society of Chemistry be held responsible for any errors or omissions in this Accepted Manuscript or any consequences arising from the use of any information it contains.

Polyphosphate coacervate gels for manufacturing of manganese loaded glass powders and fibres: structural, cytocompatibility and surface bioactivity study

Chiara Cavazzoli,^{a,b} Roberto Di Pasquale,^a Zarin Moghaddam,^a Zhao Hongjuan,^{a,c} Agron Hoxha,^a Lauren Lewendon,^a Monica Felipe-Sotelo,^a Carol Crean,^a Alfonso Zambon,^b Gigliola Lusvardi,^b Jorge Merino-Gutierrez,^{a,c} Daniela Carta^a

^a School of Chemistry and Chemical Engineering, University of Surrey, GU2 7XH, Guildford, United Kingdom.

^b Department of Chemical and Geological Sciences, Modena, University of Modena and Reggio Emilia, Italy.

^c School of Biosciences, University of Surrey, GU2 7XH, Guildford, United Kingdom.

**Corresponding author: Dr D. Carta, Email: d.cart@surry.ac.uk. Phone: +44 (0)1483 689587*

Abstract

Phosphate-based glasses (PGs) are promising bioresorbable materials for controlled delivery of therapeutic species and tissue regeneration. The traditional method of synthesis of PGs involves the use of high temperatures, which limits their biomedical applications. The main goal of this work was to manufacture Mn loaded PGs for bone regeneration using an alternative, versatile and sustainable manufacturing technique. In this work, the novel room-temperature, water-based method of coacervation was used for the synthesis of PGs in the system P_2O_5 -CaO-Na₂O-(MnO)_x where $x = 0, 1, 3, 5, 10$ mol % both in powder (PGPs) and fibre (PGFs) form. PGPs were manufactured by vacuum drying polyphosphate coacervate gels and PGFs by electrospinning them.



The addition of Mn^{2+} , which plays an important role in bone mineralization, represents a clear novelty of this work as Mn loaded PGs prepared via coacervation have not been presented to date. Mn^{2+} release in deionized (DI) water has been shown to increase with Mn^{2+} loading in both PGPs and PGFs, demonstrating tailored release by modifying its content in the glass.

In vitro biocompatibility was investigated for both systems via MTT assay on human osteosarcoma cells (MG-63) at three different ratios of dissolution products to cell medium after 24 h immersion in DI water (1, 3 and 5 % v/v). Results have demonstrated that PGPs and PGFs loaded with Mn^{2+} up to 1 mol % are the most promising systems as they are not cytotoxic at all ratios investigated. Preliminary bioactivity tests performed by immersing a PGP sample containing 1 mol % of Mn^{2+} in both cell medium (McCoy's 5A) and Tris-buffer solution for 24 and 72 h suggest the deposition of a disordered, possibly hydroxyapatite-like phase on the surface of the glass. This study demonstrates that PGPs and PGFs, synthesised via coacervation, exhibit controlled release of the therapeutic ion Mn^{2+} and promising biocompatibility, making them suitable candidates for applications such as bone regeneration and controlled delivery of therapeutic species.

Keywords: phosphate glasses; bone regeneration; coacervation, bioglasses



1. Introduction

Improvement in the quality of biomaterials for regeneration or repair of hard and soft tissues and for targeting degenerative diseases has become necessary as human life expectancy has increased significantly in the past decades. Osteoporosis and bone diseases are dramatically affecting the life of an increasing number of people, especially among the aged. As a result, the major clinical applications of biomaterials are in the field of orthopaedics (*e.g.* bone platelets, joint replacements, fixation screws) and drug delivery (*e.g.* antibiotics, antimicrobial agents). This work focuses on the use of bioresorbable glasses as biomaterials for bone regeneration. Currently, only a limited range of bioresorbable polymers is commercialised and used in medical devices and implantable carriers for drug delivery. However, their degradation often results in crystalline fragments with heterogeneous chain-lengths that could lead to toxicity.¹

In recent years, there has been an increased interest in the application of glass materials for the regeneration of damaged tissues.² The most common glasses studied for biomedical purposes are silicate-based; due to their relatively poor solubility, they are generally used to manufacture long-term implants, that could cause inflammatory reactions in the long term.³ Phosphate-based glasses (PGs) are bioresorbable materials alternative to silicate-based glasses; they have the potential to simultaneously degrade by releasing therapeutic molecules (*e.g.* antibacterial ions and anticancer drugs) and to induce tissue regeneration.^{3,4} PG powders (PGPs) and PG fibres (PGFs) in the ternary system P_2O_5 -CaO- Na_2O have been shown to have great potential as biomaterials for hard and soft tissue regeneration.^{5,6} The addition of Therapeutic Metallic Ions (TMIs) such as Ag^+ , Cu^{2+} , Zn^{2+} and Ga^{3+} to this ternary system has also been shown to imbue additional properties to PGs, such as antibacterial activity, osteogenic and angiogenic properties.^{4,6}

The morphology of PGs is crucial for tailoring them to specific applications. PGFs, which closely mimic the composition of the extracellular matrix (ECM), are suitable for soft tissue engineering applications, where the tissue has a high degree of anisotropy, such as muscle, ligaments and tendons;



however, PGFs could also be used as bone fillers and dental implants given that they can be easily packed in a localised defect.^{5–7}

The traditional method to prepare PGPs, melt-quenching (MQ), requires melting of oxide powders at temperatures $>1100\text{ }^{\circ}\text{C}$, followed by rapid cooling; PGFs are usually prepared using the conventional MQ followed by spinning of the melt (melt spinning technique, MS).^{6,8,9} However, MQ cannot be used for embedding temperature-sensitive molecules during their synthesis.^{2,7} PGs prepared via MQ have been extensively studied, in particular for hard tissue regeneration (*e.g.* promotion of osteoblast proliferation).¹⁰ The sol-gel technique (SG) is often proposed as a lower temperature alternative technique to MQ; however, this technique requires the use of alkoxide precursors, which are air-sensitive and need to be dissolved in organic solvents. Moreover, gelation times can be lengthy.¹⁰ In this work, PGs were prepared using the method of coacervation, a fast, room temperature, water-based technique.¹⁰ The coacervate method provides an attractive alternative to the MQ and SG routes, as it is sustainable and cost efficient. In addition, coacervation allows the inclusion of thermolabile drugs that can be released in a controlled manner, widening the range of biomedical applications.¹¹ Coacervation occurs when a solution of bivalent cations such as Ca^{2+} , Mg^{2+} , Zn^{2+} , Mn^{2+} , Cu^{2+} is slowly added to an aqueous solution of sodium polyphosphate. Upon addition, a phase separation occurs with the formation of a homogeneous gel-like bottom phase composed of polyphosphate chains (coacervate gel) and a supernatant aqueous layer.¹¹ The coacervate gel is formed by electrostatic interaction between the polyphosphate chains and the bivalent cations.¹¹ The gel is then separated from the supernatant aqueous layer and dried in a vacuum desiccator at room temperature to obtain a glass powder or electrospun to obtain fibres. Electrospinning (ES) is a simple, versatile and cost-effective voltage-driven process for production of fibres. The applied voltage, flow rate, nozzle to collector distance and nozzle's size determine morphology and characteristics of the electrospun fibres. ES presents several advantages over MS; it allows a high degree of control over



PGFs diameters, incorporation of thermolabile molecules, and use of injectable gel precursors prepared at room temperature instead of high temperature melts.

Very little work has been presented on glasses prepared via coacervation, particularly for biomedical applications. Only very few coacervate-made PGPs and PGFs systems loaded with silver, copper, zinc and iron ions have been presented.^{3,9,12–14} PGPs and PGFs containing silver ions demonstrated antibacterial activity against *Staphylococcus aureus* and *Escherichia coli*; furthermore, silver loaded PGFs promoted 84 % wound closure within 48 h.^{3,9} PGFs containing 10 mol % of zinc ions exhibited strong antibacterial activity against *Staphylococcus aureus*, while PGFs loaded with iron ions significantly accelerated *ex vivo* healing in chronic patient wound models, achieving over 30 % improvement in 48 h.⁹ Additionally, PGPs and PGFs loaded with copper ions and PGPs loaded with zinc ions showed excellent cellular compatibility with human osteosarcoma cells (MG-63) and human keratinocytes (HaCaTs).^{12,13}

No previous investigation has been performed on PGs containing Mn^{2+} as a TMI prepared via coacervation. Mn^{2+} is a co-factor for a broad range of enzymes (*e.g.* oxidoreductases, transferases) and it is essential in the detoxification of superoxide free radicals.⁴ Some studies have shown that Mn^{2+} has a positive effect on bone regeneration; in particular, when embedded in a silicate-based glass it has been shown to promote osteogenic differentiation, cell adhesion, ECM remodelling, osteoblast growth and osteogenic activity;^{2,15} when embedded in calcium phosphate ceramics, it has been shown to improve bone mineralization.¹⁶ An *in vitro* cytocompatibility study using osteoblast-like cells (MC3T3-E1) on Mn^{2+} embedded in hydroxyapatite (HA), has demonstrated that Mn^{2+} improved cell adhesion.¹⁷ It has been reported in the literature that manganese ions can form P–O–Mn linkages with phosphate groups, strengthening the phosphate glass network.¹⁸

In this work, PGPs and PGFs in the system $\text{P}_2\text{O}_5\text{-CaO-Na}_2\text{O-(MnO)}_x$ ($x = 0, 1, 3, 5, 10$ mol %) were prepared via coacervation: the rheology of the coacervate gels, the structure of PGPs and PGFs, and their dissolution properties over time were investigated.



Cell viability data on human osteosarcoma cells MG-63 in contact with both PGPs and PGFs dissolution products obtained after 24 h immersion in DI water, have shown good cytocompatibility at three different ratios of dissolution products to cell medium (DP-CM): 1, 3, 5 % v/v. The most promising sample in terms of biocompatibility was then tested for *in vitro* bioactivity.

In vitro bioactivity of SG-made silicate-based glasses is usually demonstrated by the formation of bone-like phases on their surfaces (*e.g.* HA or HCA hydroxycarbonate apatite), when in contact with simulated body fluid (SBF), Tris-HCl buffer or cell media.^{19–22} However, the formation of phases that could promote bone regeneration on the surface of PGs has been reported to be challenging, with some studies reporting inhibition of HA formation from polyphosphates and pyrophosphates systems.²³ Conflicting results on the formation of HA on the surface of PGs have been reported after immersion in SBF.^{19,24} Some studies indicate no formation at all,²⁵ while others report HA formation only after very long immersion times (20–28 days).^{26–28} Recently, Kumar *et al.*²⁹ reported that the $\text{Zr}_{12}\text{Ca}_{18}\text{P}_{70}$ bioglasses, synthesized via MQ, are capable of forming a HA layer on their surface after 30 days of immersion in SBF; however, this behaviour seems to be related to the presence of Zr^{4+} on the PGs's surface. It has been reported that the formation of bone-like phases on silicate-based glasses occurs faster when using Tris-buffer instead of SBF.^{19,21} This has been ascribed to the presence of Mg^{2+} in the SBF medium, which is then incorporated into the apatite lattice instead of Ca^{2+} .^{21,30} Therefore, in this work, Tris-HCl buffer and McCoy's 5A (M5A) cell medium (CM) were chosen for investigating the bioactivity of a selected Mn loaded coacervate PGP upon immersion.

2. Experimental

2.1. Synthesis of coacervate PGPs and PGFs

In order to prepare the ternary PGs P_2O_5 -CaO- Na_2O , 20 mL of a 2 M aqueous solution of calcium nitrate tetrahydrate ($\text{Ca}(\text{NO}_3)_2 \cdot 4\text{H}_2\text{O}$, Thermo Scientific, 99.0%), obtained by dissolving 47.23 g of $\text{Ca}(\text{NO}_3)_2 \cdot 4\text{H}_2\text{O}$ in 100 mL of water, was slowly added to 20 mL of a 0.16 M aqueous solution of



sodium polyphosphate (NaPP, $(\text{NaPO}_3)_n$; Merck, 99.0%, $n \sim 25$), obtained by dissolving 40.78 g of NaPP in 100 mL of water, using a syringe pump (20 mL/h) under constant and vigorous stirring. During addition, a phase separation occurred in which an upper aqueous layer and a lower coacervate layer formed. The mixture was stirred for 1 h and allowed to settle for 24 h.

The bottom layer (coacervate gel) was then isolated and dried in a vacuum desiccator at room temperature for 24 h to obtain a dry glass powder, PGP. To obtain PGFs, the coacervate gels were transferred into a plastic syringe and electrospun; upon application of a high voltage (15 kV), the gels were ejected from the nozzle of the electrospinner, and PGFs were deposited on a metal screen collector.

In order to prepare the quaternary PGs $\text{P}_2\text{O}_5\text{-CaO-Na}_2\text{O-(MnO)}_x$ ($x = 1, 3, 5, 10$ mol %), 0.6, 1.8, 3.0 and 6.0 mL, respectively of a 2 M aqueous solution of manganese (II) nitrate tetrahydrate ($\text{Mn(NO}_3)_2 \cdot 4\text{H}_2\text{O}$; Fluka™, 97.0%), obtained by dissolving 7.53 g of $\text{Mn(NO}_3)_2 \cdot 4\text{H}_2\text{O}$ in 15 mL of water, was added dropwise with vigorous stirring following the complete addition of $\text{Ca(NO}_3)_2 \cdot 4\text{H}_2\text{O}$ to the 0.16 M NaPP solution and allowed to settle for 24 h. The gels were then isolated and dried in a vacuum desiccator at room temperature or electrospun to obtain fibres as previously described for the ternary systems.

A schematic of the coacervation method for the production of coacervate gels is shown in Figure 1A, and images of all coacervate gels prepared in this work are shown in Figure 1B. A representative image of a PGP obtained after vacuum drying the ternary coacervate gel for 24 h is shown in Figure 1C; the cotton-like bundle of PGFs obtained after ES of the same gel are shown in Figure 1D.

Gels, powders and fibres will be hereafter named as Gel-MnX, PGP-MnX, and PGF-MnX, respectively, where X is the mol % of Mn^{2+} (0, 1, 3, 5, 10).



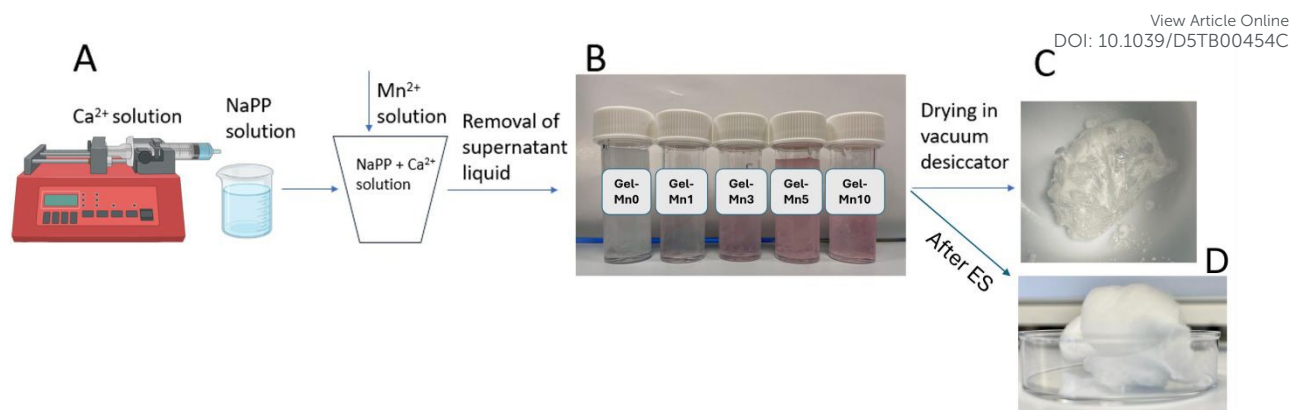


Figure 1. (A) Schematic of the synthesis of PGs via coacervation; (B) images of all coacervate gels; (C) PGP-Mn0 in the system P_2O_5 -CaO- Na_2O obtained after drying of the coacervate Gel-Mn0 in a vacuum desiccator; (D) cotton-like bundle of PGF-Mn0 after ES of Gel-Mn0.

2.2. Electrospinning of coacervate gels

ES is a technique employed to produce fibres from a liquid precursor by applying a high voltage between the emitter nozzle and a grounded collector. As the precursor solution is fed through the emitter, it acquires an electric charge and is attracted toward the oppositely charged collector. Initially, a Taylor cone is formed at the nozzle tip due to the balance between electrostatic repulsion and surface tension. When the applied voltage exceeds a critical threshold, a continuous jet of the charged liquid is ejected, which elongates and solidifies into a fine fibre. The resulting fibre diameter can be tuned by adjusting parameters such as the flow rate, applied voltage, and the viscosity of the precursor solution.

In this work, ES was performed at room temperature using a stainless-steel capillary (gauge 18 nozzle), syringe pump, and high voltage source (Spraybase system, Kildare). The distance between the capillary tip and the collector was set at 15 cm, the flow rate was set at 2.0 ml/h and a voltage of 15 kV was applied between the nozzle and a metal screen collector, where PGFs were deposited and



collected. These conditions were chosen based on previous work on PGFs in the system $\text{P}_2\text{O}_5\text{-CaO}$ loaded with Ag^+ , Zn^{2+} , Fe^{3+} and Ga^{3+} .^{9,14}

2.3 Rheology

Viscosity of coacervate gels was measured from a shear rate of 0.1 to 100 $\text{rad} \cdot \text{s}^{-1}$ using an MCR 92 rheometer (Anton Paar) equipped with a 50 mm diameter parallel plate at 20 °C, using 30 s of equilibration. Measurements were performed in triplicate. Analysis was performed straight after the removal of the supernatant liquid from the top of the coacervate gels, to avoid possible hydrolysis of the polyphosphate chains.³¹

2.4. Structural and morphological characterisation of PGPs and PGFs

X-Ray Powder Diffraction (XRPD) was performed using a PANalytical X'Pert diffractometer (Royston, UK) in a flat plate geometry using a Ni filtered $\text{Cu-K}\alpha$ radiation. Data were collected using a PIXcel-1D detector with a step size of 0.0525° and a time per step of 12 s over an angular range of $2\theta = 20\text{--}90^\circ$.

Fourier Transform Infrared (FT-IR) spectra were collected using a Perkin Elmer spectrometer 2000-FT-IR (Seer Green, UK) in the range of $4000\text{--}400\text{ cm}^{-1}$. Raman spectroscopy was performed in the range of $600\text{--}1300\text{ cm}^{-1}$ using a 532 nm laser as a source. A Thermo Fisher Scientific DXR3 Raman microscope with a 10 mW was used for PGPs, and a Renishaw InVia Reflex Raman Microscope with a 50 mW was used for PGFs (2400-line grating).

Scanning electron microscopy (SEM) was performed using an APREO SEM at an accelerating voltage of 15 kV. PGs were mounted onto an aluminium stub using carbon conductive tape. EDX was performed on PGPs and PGFs after vacuum drying using a WDS MagnaRay spectrometer (Hemel Hempstead, UK) mounted on an APREO SEM.



2.5. Dissolution studies

View Article Online
DOI: 10.1039/D5TB00454C

To assess the species released upon dissolution, 10 mg of each PGP and PGF was immersed in 10 mL of deionized (DI) water (Veolia Water, Elga Centra, resistivity 18.2 M Ω ·cm) and left in an incubator at 37 °C under shaking at 190 rpm. The solutions containing dissolution products released by PGs were collected at different time points following immersion (3, 24, 48 and 72 h). Dissolution tests were performed in triplicates (n = 3). At each time point, the resulting suspensions were centrifuged at 4800 rpm for 5 minutes to separate the undissolved PGs from the solutions to be analysed. The dissolution products were then filtered with a 0.45 μ m unit (Millipore filter unit, Millex™-GP) and diluted 1:50 with 2% v/v nitric acid (HNO₃ for Trace Metal Analysis, Fisher Chemical), prior to analysis of P, Ca, Na, Mn using microwave plasma atomic emission spectroscopy (MP-AES, Agilent 4210). For quantitative purposes, the instrument was calibrated daily with a set of standards (Aristar, Fisher Scientific, UK), diluted in 2 % v/v HNO₃ within the range from 0.01 to 10 μ g·mL⁻¹ for Na, Ca and P, and from 0.1 to 10 μ g·mL⁻¹ for Mn. A solution of 5 μ g·mL⁻¹ of Be was used as internal standard to correct for any sensitivity drifts during analysis. Emission of the analytes was recorded at the wavelengths 588.995, 393.366, 213.618, and 403.076 nm, for Na, Ca, P and Mn, respectively.

2.6. Cell viability tests

Cell viability was assessed via total mitochondrial dehydrogenase activity. Enzyme activity was determined using the 3-(4,5-dimethylthiazol-2-yl)-2,5-diphenyl tetrazolium bromide (MTT) assay (Sigma-Aldrich).³² Toxicological effect of PGPs and PGFs' dissolution products on human osteosarcoma cell line MG-63 (LGC ATTC-CRL-1427) was tested using different ratios of dissolution products (products obtained after dissolution of PGs at different time points) to cell medium. MG-63 cells were cultured in DMEM with 10% v/v foetal bovine serum (Gibco, Invitrogen) and 100 U mL⁻¹ of penicillin/streptomycin (Gibco, Invitrogen) in a humidified incubator at 5% CO₂



and 37 °C. Cells were routinely passaged at 80–90% of confluence. 100 µL of the cell suspension were then seeded into 96-well plates at a density of 30,000 cells per well and incubated with DMEM for 24 h.

A series of stock solutions of the 24 h PGPs and PGFs' dissolution products and cell medium (DMEM with 2% v/v foetal bovine serum) were prepared at 1, 3 and 5% v/v ratio. The 1% stock solution was prepared by adding 5 µL of dissolution products to 495 µL of cell medium. Similarly, 15 µL and 25 µL of dissolution products were mixed with 485 µL and 475 µL, respectively, to prepare 3% and 5% stock solution. The controls were treated with cell medium only. 100 µL of each stock solution were applied to treat the cells. Each treatment option was performed in triplicate. The behaviour of the MG-63 cells in these environments was monitored.

After 24 h incubation, 10 µL of MTT (1 mg mL⁻¹ in phosphate-buffered saline solution) were added in each well before continuing incubation for 3 h. 100 µL DMSO (Sigma-Aldrich) per well were then added after media were aspirated. The plates were incubated at room temperature for 30 min before measuring the absorbance at 570 nm with a CLARIOstar microplate-reader (BMG Labtech). Absorbance was then used to calculate the cell viability using the equation % cell viability = (absorbance of treated cells / absorbance of control cells) x 100.

2.7. *In vitro* bioactivity assessment

For studying the *in vitro* bioactivity of dissolution products of the selected PGP-Mn1 sample, two different types of media were used: Tris-HCl buffer (Tris-B) solution and cell medium (M5A).²¹ The Tris-B solution was prepared by first dissolving 15.09 g of tris(hydroxymethyl)aminomethane (Sigma-Aldrich) in 1.5 L of DI water, followed by the addition of 44.2 mL of 1 M hydrochloric acid (HCl, Sigma-Aldrich); the solution was then kept in a 37 °C incubator overnight. The pH was adjusted to 7.3 using 1 M HCl before diluting the solution up to a total volume of 2 L with DI water. The



solution was stored in an incubator at 37 °C before use. The M5A medium containing 1.5 mM of L-glutamine and 2200 mg mL⁻¹ sodium bicarbonate (ThermoFisher) was used as purchased.

To test the bioactivity, 75 mg of the selected PGP sample were immersed in 50 mL of Tris-B and M5A and stored in an incubator at 37 °C, while shaking at 190 rpm for 24 and 78 h. The powders were then filtered using a paper filter (LLG-Plain disc filter, diameter = 125 mm), washed with DI water and dried at 37 °C overnight. The dry powders were then characterised using XRPD, FT-IR and SEM.

3. Results

3.1. Rheology of polyphosphate coacervate gels

Viscosity and shear stress of all coacervate gels were measured as a function of shear rate in the range 0.1 to 100 rad · s⁻¹ (Figure 2A and 2B, respectively). All gels exhibit a Newtonian flow behaviour, as indicated by the constant viscosity observed across the entire shear rate range measured (Figure 2A). This suggests that the gels maintain a consistent internal resistance to flow regardless of shear rate. This is also shown by the linear relationship between shear stress and shear rate (Figure 2B). The gels behaviour can be described by the Herchel-Bulkley equation: $\tau = \tau_0 + k \times \gamma^n$, where τ represents the shear stress, τ_0 is the yield stress, k is the consistency factor, γ is the shear rate and n is the flow index. For Newtonian fluids, the flow index (n) equals 1, leading to a linear relationship between shear stress and shear rate ($\tau = \tau_0 + k \times \gamma$).



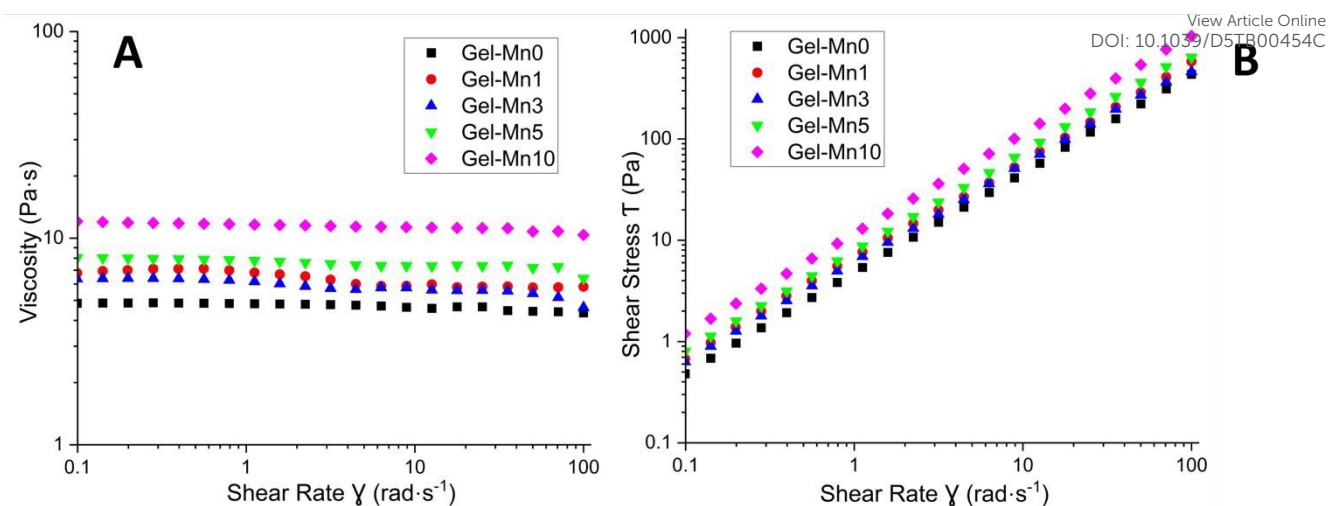


Figure 2. Viscosity vs shear rate (A) and shear stress vs shear rate (B) of all polyphosphate coacervate gels.

Table 1 shows the viscosity values for all gels measured at a very low shear rate (0.1 rad s^{-1}) along with the consistency factors k . A general trend in increasing viscosity with increasing the Mn loading can be identified; the viscosity for Gel-Mn0 is $5.20 \pm 0.30 \text{ Pa} \cdot \text{s}$ and $13.77 \pm 2.80 \text{ Pa} \cdot \text{s}$ for Gel-Mn10.

Table 1. Viscosities at shear rate 0.1 rad s^{-1} and consistency factors (k) for all polyphosphate coacervate gels.

Sample	Viscosity ($\text{Pa} \cdot \text{s}$)	k
Gel-Mn0	5.20 ± 0.30	5.07 ± 0.49
Gel-Mn1	6.74 ± 0.16	6.02 ± 0.18
Gel-Mn3	5.83 ± 0.38	5.06 ± 0.13
Gel-Mn5	8.67 ± 1.14	7.07 ± 0.53
Gel-Mn10	13.77 ± 2.80	12.77 ± 2.94



3.2. XRPD and SEM/EDX

View Article Online
DOI: 10.1039/D5TB00454C

Upon vacuum drying and electrospinning of the polyphosphate gels, PGPs and PGFs are obtained, respectively. In order to assess the absence of crystallinity, XRPD patterns of all PGPs and PGFs were recorded in the 2θ range of 20 – 90° (Figure 3A and 3B, respectively). No Bragg peaks were observed in any of the samples, indicating that all of them are amorphous. The broad halo observed at $2\theta \sim 28^\circ$ in both systems can be ascribed to the amorphous phosphate network.

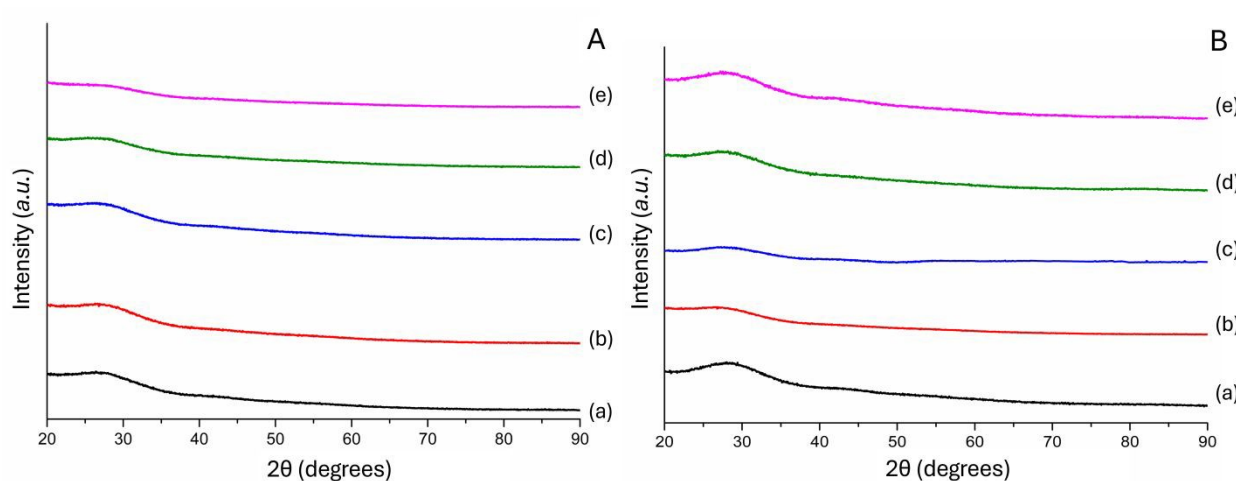


Figure 3. XRPD patterns of A): (a) PGP-Mn0; (b) PGP-Mn1; (c) PGP-Mn3; (d) PGP-Mn5; (e) PGP-Mn10 and B): (a) PGF-Mn0; (b) PGF-Mn1; (c) PGF-Mn3; (d) PGF-Mn5; (e) PGF-Mn10.

The composition of PGPs and PGFs was evaluated using SEM equipped with an EDX detector. Even though the quantification of oxygen via EDX suffers from the fact that it is a light element, compositions in terms of oxides can be calculated considering the expected oxides stoichiometries. Compositions expressed as mol % of oxides, are presented in Table 2 (compositions expressed as atomic % of each element are reported in Table SI-1). The P_2O_5 , CaO, Na_2O and MnO content of these PGs obtained by EDX are in good agreement with previous work on coacervate-made PGs.^{14,33} P_2O_5 content varies between ~ 50 and 57 mol % for PGPs and between ~ 54 and 62 mol % for PGFs. CaO and Na_2O content decreases by increasing Mn loading in both PGPs and PGFs. CaO is in the



range of ~ 33 - 40 mol % and ~ 22 - 35 mol %, and Na₂O is in the range of ~ 5 - 10 mol% and ~ 3
12 mol % for PGPs and PGFs, respectively. MnO content varies between ~ 1 and 11 mol % and ~ 1
and 12 mol%, for PGPs and PGFs, respectively. Previous works^{34–36} show that glasses with CaO
content in the range ~ 20 - 40 mol% have good biocompatibility and bioactivity.

Table 2. Compositions of PGPs and PGFs expressed in mol % of oxides measured via EDX.

Sample	P ₂ O ₅	CaO	Na ₂ O	MnO
PGP-Mn0	50.2 ± 0.4	39.7 ± 0.2	10.0 ± 0.2	-
PGP-Mn1	57.3 ± 0.4	32.5 ± 0.5	9.2 ± 0.3	1.0 ± 0.3
PGP-Mn3	50.1 ± 0.3	37.1 ± 0.2	9.8 ± 0.4	3.0 ± 0.5
PGP-Mn5	51.9 ± 0.4	34.2 ± 0.5	8.9 ± 0.5	5.0 ± 0.4
PGP-Mn10	51.0 ± 0.5	32.8 ± 0.4	5.2 ± 0.2	10.9 ± 0.4
PGF-Mn0	54.4 ± 0.8	34.5 ± 0.3	11.1 ± 0.5	-
PGF-Mn1	57.3 ± 0.5	30.0 ± 0.4	11.6 ± 0.2	1.1 ± 0.4
PGF-Mn3	59.1 ± 0.4	28.4 ± 0.5	9.1 ± 0.4	3.4 ± 0.2
PGF-Mn5	60.5 ± 0.7	28.8 ± 0.2	4.6 ± 0.4	6.1 ± 0.5
PGF-Mn10	62.1 ± 0.9	22.3 ± 0.4	3.3 ± 0.8	12.3 ± 0.3

SEM images of PGPs show smooth surfaces particles in the range 60-80 µm in size. A representative SEM image of PGP-Mn1 is shown in Figure SI-1. SEM images of PGFs confirm the presence of fibres with an average diameter of ~ 3 µm (Figure 4). It has to be noted that as Mn loading increases, an increased number of smaller PGFs can be observed (Figure 4 D-E).

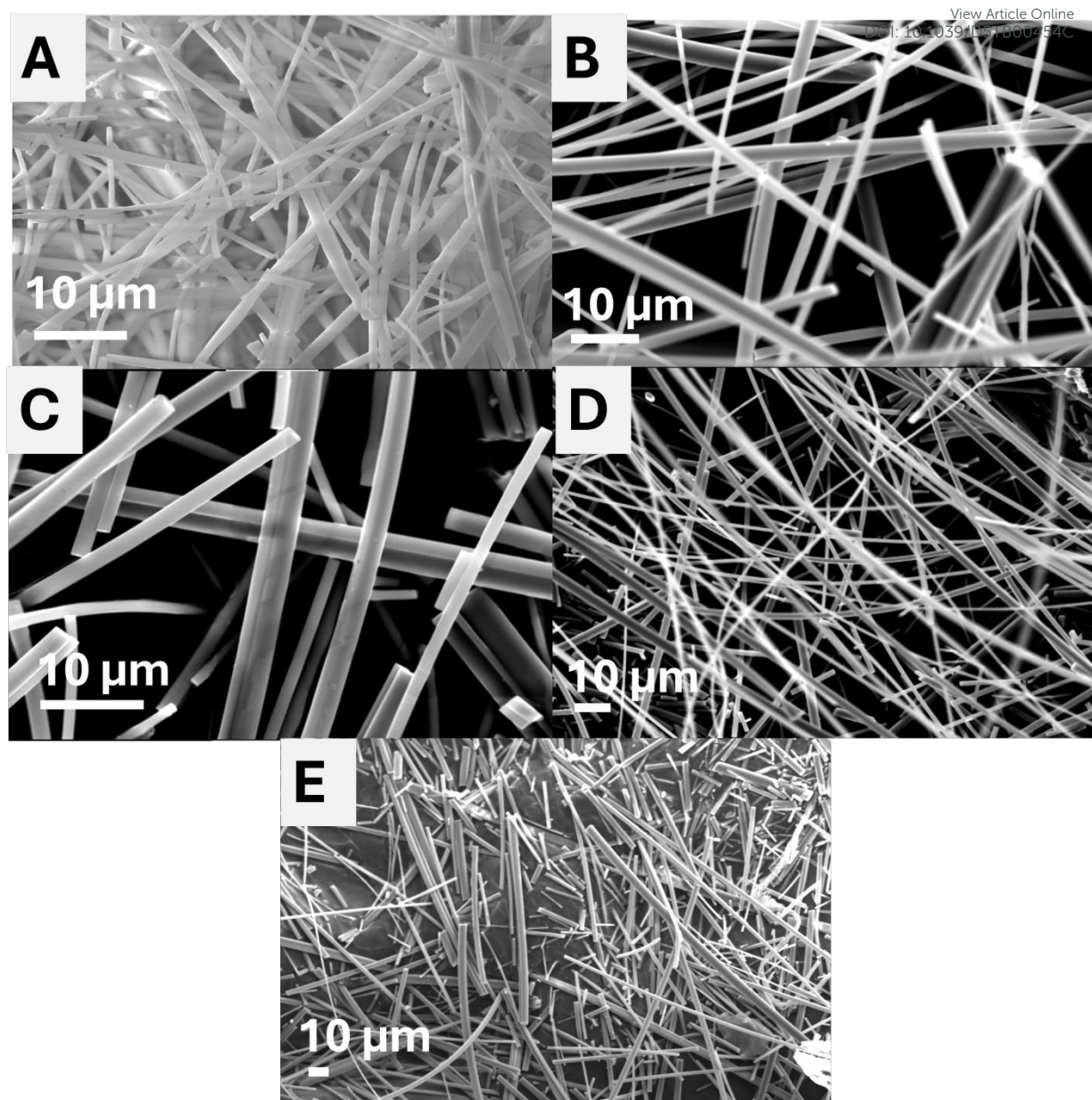


Figure 4. SEM images of (A) PGF-Mn0, (B) PGF-Mn1, (C) PGF-Mn3, (D) PGF-Mn5, (E) PGF-Mn10.

3.3. FT-IR and Raman spectroscopies

The structure of PGPs and PGFs network was studied by FT-IR and Raman spectroscopies (Figure 5 and 6, respectively). Qualitative identification of main vibrational groups and assignment of the

principal phosphate vibrational modes has been performed. Phosphate network connectivity will be described using the Q^n notation, where n indicates the number of bridging oxygens. The broad bands observed in all spectra are consistent with the amorphous nature of all samples.

FT-IR spectra of PGPs (Figure 5A) and PGFs (Figure 5B) look very similar. Peak assignment was performed according to previous studies on PGs.^{11,13,37,38}

The in-chain, (P-O-P) Q^2 groups give rise to the bands at $\sim 490\text{ cm}^{-1}$ corresponding to the bending mode $\delta(\text{P-O-P})$; the band at $\sim 900\text{ cm}^{-1}$ assigned to the asymmetric stretching $\nu_{\text{as}}(\text{P-O-P})$ and the less intense band at $\sim 725\text{ cm}^{-1}$ corresponding to the symmetric stretching $\nu_{\text{s}}(\text{P-O-P})$.

The out-of-chain $Q^2\text{PO}_2$ groups give rise to the bands at $\sim 1240\text{ cm}^{-1}$ corresponding to the asymmetric stretching mode of $\nu_{\text{as}}(\text{PO}_2)^-$. Finally, the band at $\sim 1100\text{ cm}^{-1}$ corresponds to the asymmetric stretching modes of chain-terminating, Q^1 groups, $\nu_{\text{as}}(\text{PO}_3)^{2-}$.

The full range FT-IR spectra measured up 4000 cm^{-1} reported in Figure SI-2 show the bands $\sim 3400\text{ cm}^{-1}$ in addition to the band at ~ 1640 that can be assigned to the bending and stretching of O-H bonding of residual water.

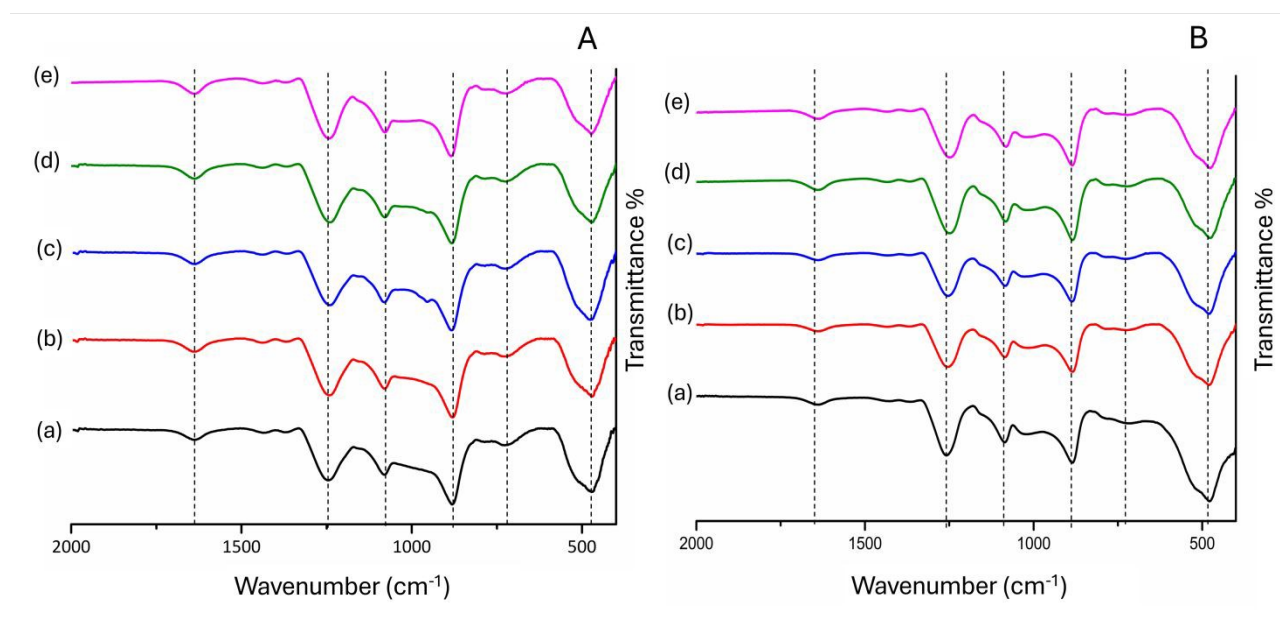


Figure 5. FT-IR spectra of A): (a) PGP-Mn0; (b) PGP-Mn1; (c) PGP-Mn3; (d) PGP-Mn5; (e) PGP-Mn10 and B): (a) PGF-Mn0; (b) PGF-Mn1; (c) PGF-Mn3; (d) PGF-Mn5; (e) PGF-Mn10.



Poor resolution affects FT-IR measurements due to the broadness of the peaks, which often results in little difference between spectra of different compositions.³⁹ Therefore, Raman spectra of all PGPs and PGFs were also collected and shown in Figures 6A and 6B, respectively. Same Q^n notation used for FT-IR is used to describe the connectivity of the phosphate network.

Raman spectra for all compositions of PGPs are very similar and show six main bands (Figure 6A).¹² The strong band at approximately 700 cm^{-1} and the shoulder at 750 cm^{-1} are assigned to the symmetric stretching mode of in-chain Q^2 P-O-P groups, $\nu_s(\text{P-O-P})$;⁴⁰ whereas the asymmetric mode of the same Q^2 units occurs as a lower intensity band at 900 cm^{-1} , $\nu_{as}(\text{P-O-P})$. The bands around 1170 and 1250 cm^{-1} are assigned to the symmetric ν_s and asymmetric ν_{as} stretching modes of the Q^2 out-of-chain groups $(\text{PO}_2)^-$, respectively. Finally, the band at 1050 cm^{-1} can be assigned to the symmetric stretching of the Q^1 , end of chain, $\nu_s(\text{PO}_3)^{2-}$.

Raman spectra of PGFs are reported in Figure 6B. Here only four main bands are observed: the symmetric stretching mode of in-chain Q^2 groups, $\nu_s(\text{P-O-P})$ at 700 cm^{-1} (the asymmetric shoulder cannot be visualised); the symmetric stretching of the Q^1 , end of chain, $\nu_s(\text{PO}_3)^{2-}$ at 1050 cm^{-1} and the symmetric ν_s and asymmetric ν_{as} stretching modes of the Q^2 out-of-chain groups $(\text{PO}_2)^-$ at 1170 and 1250 cm^{-1} , respectively. In both systems, the absence of a strong, sharp band in the $950\text{--}1000\text{ cm}^{-1}$ region corresponding to isolated orthophosphate groups, $(\text{PO}_4)^{3-}$, suggests that orthophosphate species Q^0 are either absent or present in negligible amounts in all samples.



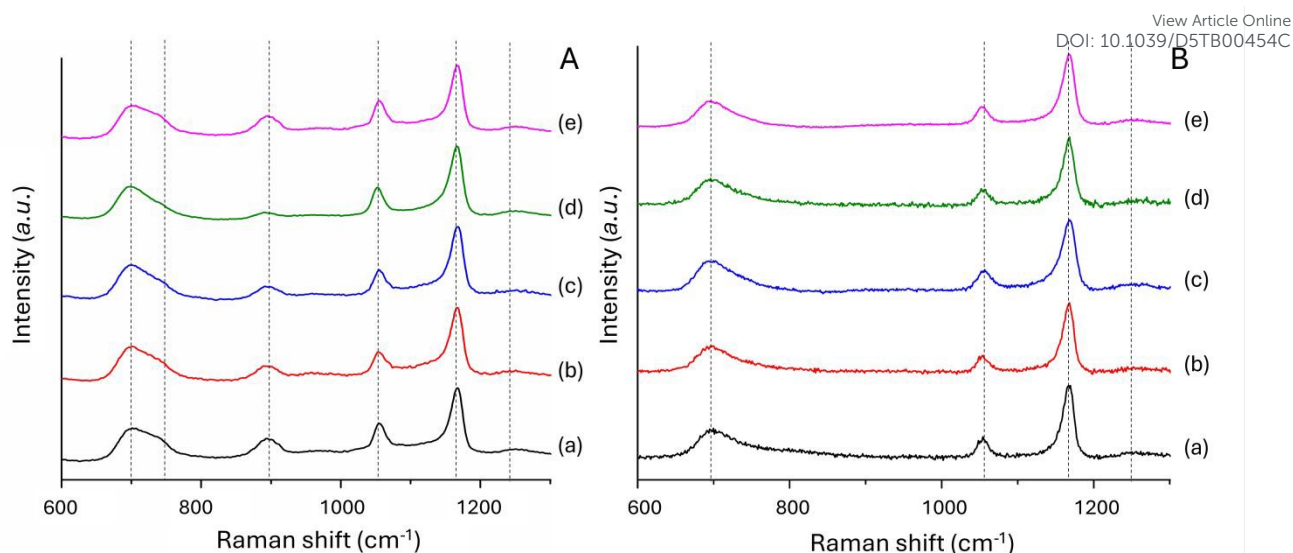


Figure 6. Raman spectra of A): (a) PGP-Mn0; (b) PGP-Mn1; (c) PGP-Mn3; (d) PGP-Mn5; (e) PGP-Mn10 and B): (a) PGF-Mn0; (b) PGF-Mn1; (c) PGF-Mn3; (d) PGF-Mn5; (e) PGF-Mn10.

3.4. Dissolution studies

Whereas dissolution studies of PGs made via MQ in DI water have been widely investigated,^{10,41} dissolution studies of coacervate PGs are scarce. Dissolution profiles of P, Ca, Na and Mn ions after immersion of PGPs and PGFs in DI water over a period of 72 h were determined using MP-AES (Figures 7 and 8). All species show a high release in the first 24 h followed by a slower release.

For all systems, PGPs and PGFs, there is a clear relationship between Mn loading and release of P and Na. As Mn loading increases, P release increases and Na release decreases, for all timepoints. The lowest release of P, after 72 h, is observed in Mn-free samples (500 and $800 \mu\text{g}\cdot\text{mL}^{-1}$ for PGP-Mn0 and PGP-Mn10, and about 150 and $300 \mu\text{g}\cdot\text{mL}^{-1}$ for PGF-Mn0 and PGF-Mn10, respectively). In contrast, the highest release of Na, after 72 h, is observed in Mn-free samples (60 – $63 \mu\text{g}\cdot\text{mL}^{-1}$ for PGP-Mn0 and PGF-Mn0 versus 40 – $44 \mu\text{g}\cdot\text{mL}^{-1}$ for PGP-Mn10 and PGF-Mn10).

Ca release remains consistent regardless of Mn loading, with all samples releasing approximately 140 – $160 \mu\text{g}\cdot\text{mL}^{-1}$ after 72 h. As expected, Mn release increases with Mn content, ranging from 10 –



11 $\mu\text{g}\cdot\text{mL}^{-1}$ in PGP-Mn1 and PGF-Mn1 to 45–49 $\mu\text{g}\cdot\text{mL}^{-1}$ in PGP-Mn10 and PGP-Mn10 after 72 h.

View Article Online
DOI: 10.1039/D5TB00454C

Despite PGPs and PGFs show similar release trends for Na, Ca and Mn, some differences are observed in the overall amount of P released over time. P release is significantly lower for PGFs than PGPs, being about 500 and 800 $\mu\text{g}\cdot\text{mL}^{-1}$ for PGP-Mn0 and PGP-Mn10, respectively and about 150 and 300 $\mu\text{g}\cdot\text{mL}^{-1}$ for PGF-Mn0 and PGF-Mn10.

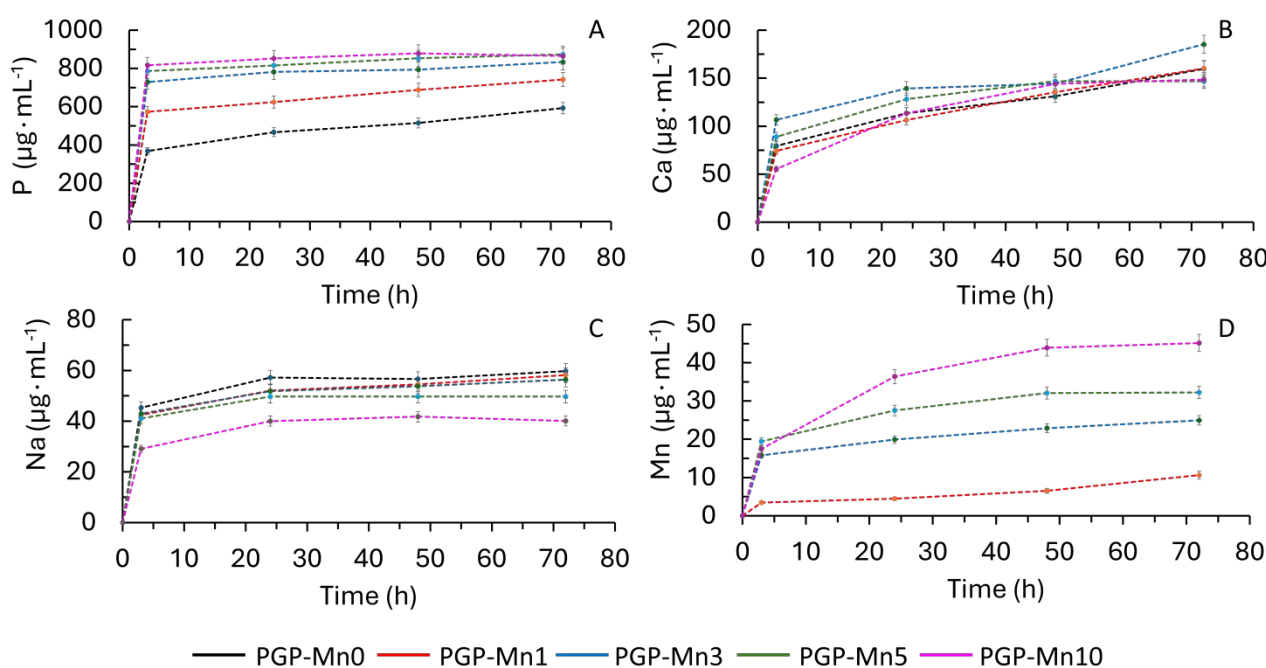


Figure 7. PGPs release of P (A), Ca (B), Na (C) and Mn (D) ions in DI water over 72 h.



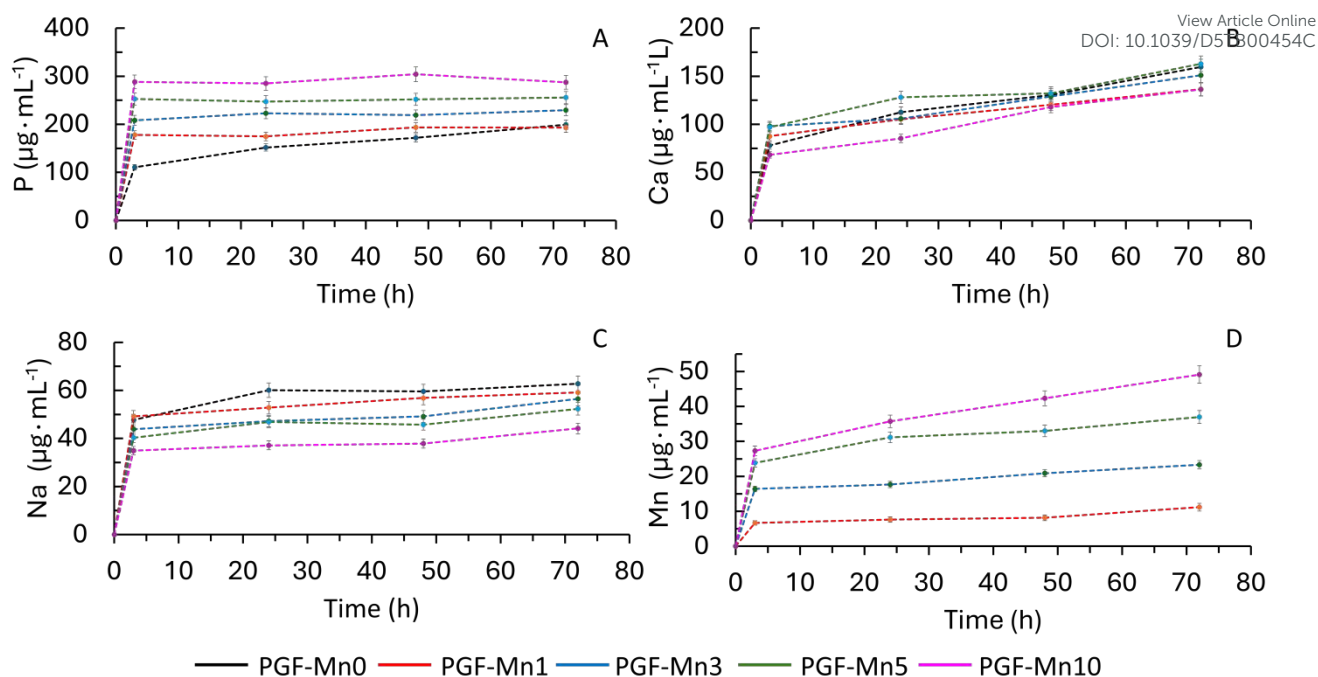


Figure 8. PGFs release of P (A), Ca (B), Na (C) and Mn (D) ions in DI water over 72 h.

3.5. Cell viability assay on MG-63

The effect of PGPs and PGFs' dissolution products on the viability of MG-63 cells was investigated using three different ratios dissolution products (obtained after 24 h immersion in DI water) to cell medium 1, 3, 5 % v/v hereafter called DP-CM1, DP-CM3 and DP-CM5, respectively. MTT viability of MG-63 cells exposed to PGPs and PGFs' dissolution products at different DP-CM ratios are shown in Figures 9A and 9B, respectively. None of the PGFs' dissolution products show a statistically significant difference in cell viability compared to the control with cell viabilities always higher than $\sim 81\%$. Only few of the dissolution products from PGPs seem to slightly decrease the viability (PGP-Mn3 at DP-CM-3 and DP-CM5 ratios and PGP-Mn10 at DP-CM-1 and DP-CM3 ratios). However, cell viability never falls under 72% for any of the PGPs' dissolution products, indicating an adequate cell response.



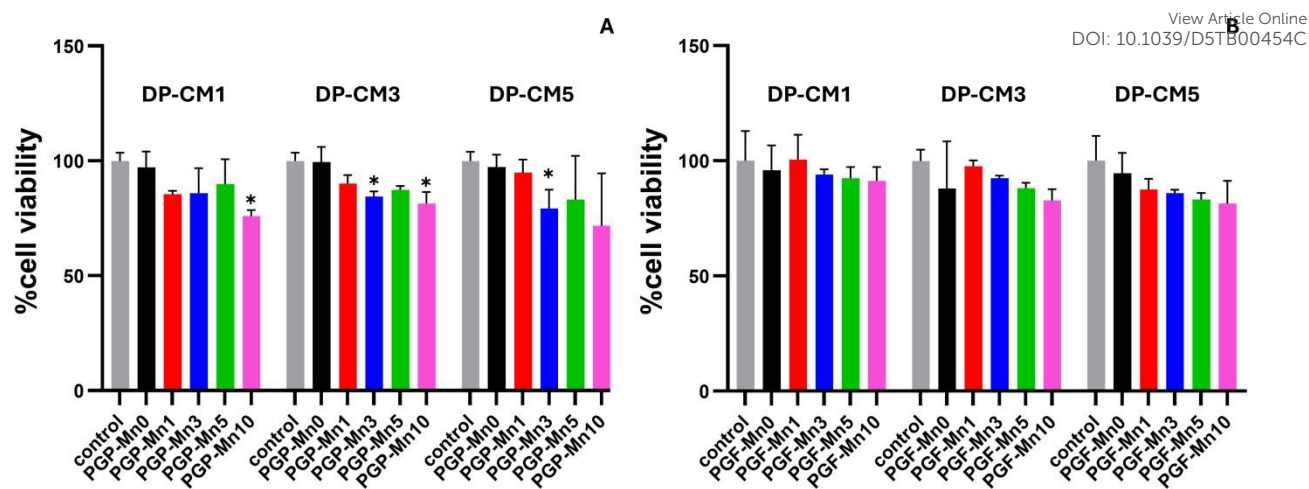


Figure 9. MTT viability of MG-63 cells exposed to dissolution products of PGPs (A) and PGFs (B) after 24 h of incubation. Two-way ANOVA was used to analyse the data. * Indicates P value less than 0.05.

For both PGPs and PGFs systems, the highest cell viability % values were observed for dissolution products deriving from PGP-Mn1 and PGF-Mn1 at every DP-CM ratio. Given that the fibrous samples show a very similar structure and similar ion release to powders, we selected only the powder sample PGP-Mn1 for exploratory bioactivity testing.

3.6. Bioactivity testing

Preliminary bioactivity testing was done by immersing the selected sample, PGP-Mn1, in Tris-B and in CM for 24 and 72 h followed by analysis of structural and morphological changes of the powder after immersion. The changes were monitored via XRPD, FT-IR and SEM.

As pH is an important parameter that affects HA formation, its value before and after immersion of PGP-Mn1 in both Tris-B and CM was measured. The pH of CM (~7.3) does not change after 24 h of being in contact with PGP-Mn1; however, it slightly decreases after 72 h to ~7.0. The pH of Tris-B is ~7.4, and remains constant after being in contact with PGP-Mn1 up to 72 h.



In Figure 10A, FT-IR spectra of PGP-Mn1 before (Figure 10A-a) and after immersion in CM (Figure 10A-b 24 h and A-c 72 h of immersion) and in Tris-B (Figure 10A-d 24 h and A-e 72 h of immersion) are presented in the range 2500 - 400 cm^{-1} . The FT-IR spectra across the entire range of 4000-400 cm^{-1} are reported in Figure SI-3. The assignation of FT-IR bands of PGP-Mn1 before immersion (Figure 10A-a) has been previously discussed. After immersion some changes can be observed.

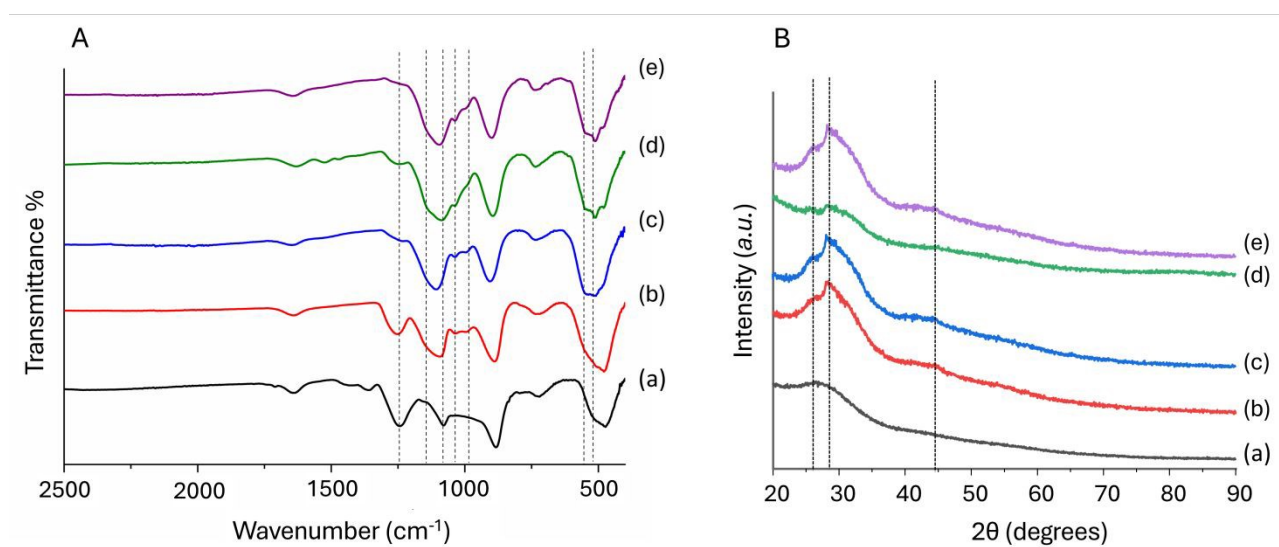


Figure 10. FT-IR spectra (A) and XRD patterns (B) of PGP-Mn1 before (a) and after immersion in CM for 24 h (b) and 72 h (c) and after immersion in Tris-B for 24 h (d) and 72 h (e).

First, the band at 1240 cm^{-1} , assigned to asymmetric stretching $\nu_{\text{as}}(\text{PO}_2^-)$, clearly seen in PGP-Mn1 before immersion, decreases in intensity after immersion in both media for 24 h and is barely visible after 72 h. This is particularly evident in the sample immersed in Tris-B where the intensity of this band is very low even after 24 h (Figure 10A-d). This is due to a decrease in out-of-chain oxygens. Two new bands at 1037 and 990 cm^{-1} and a shoulder at 560 cm^{-1} are observed after immersion in both media, even after 24h. There is also the formation of a peak at 514 cm^{-1} within the broad band at $\sim 490 \text{ cm}^{-1}$ that has been ascribed in the literature to the vibrations of $(\text{PO}_4)^{3-}$ in the Q^0 structure. The band at $\sim 1100 \text{ cm}^{-1}$ is already present before immersion, but its intensity increases,



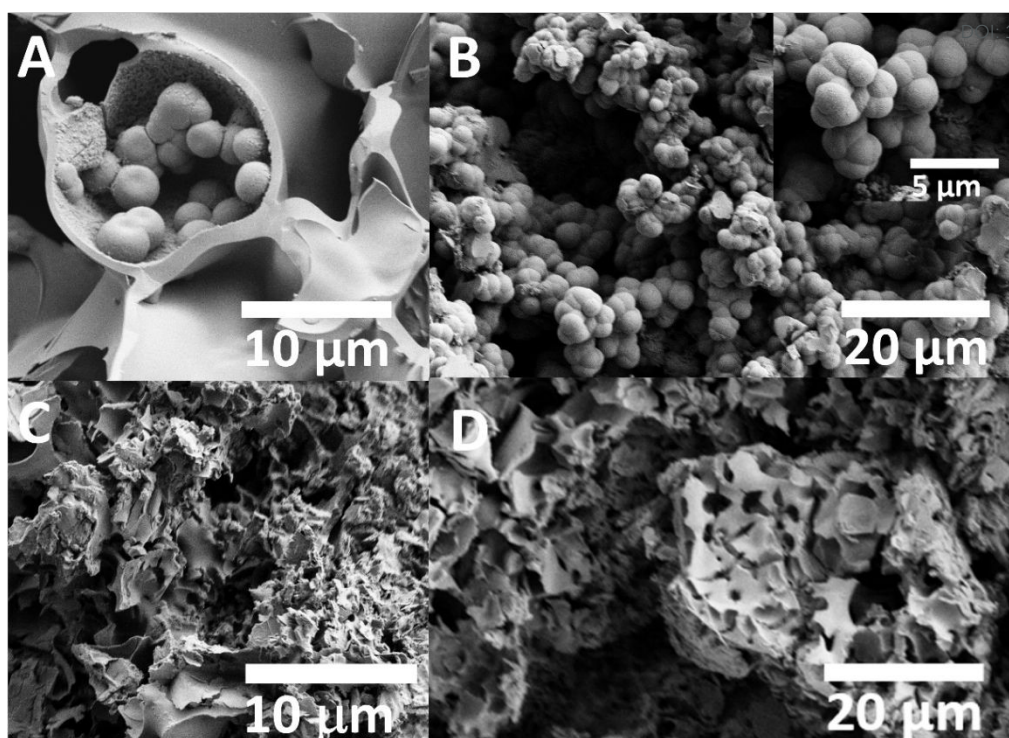
especially after 72 h. After soaking, an additional shoulder at $\sim 1140\text{ cm}^{-1}$ is observed, which is attributable to symmetric $\nu_s(\text{PO}_2^-)$ stretching mode.²⁴

Some changes in the XRPD patterns after immersion are also observed. In Figure 10B, XRPD patterns of PGP-Mn1 before immersion (Figure 10B-a) and after immersion in CM (Figure 10B – b 24 h and 10B – c 72 h of immersion) and in Tris-B (Figure 10B – d 24 h and 10B – e 72 h of immersion) are presented. Two weak peaks at $2\theta \sim 25$ and 28 degrees can be seen after 24 h of immersion in both media, overlapping the main halo due to the amorphous phosphate network centred at 28 degrees, in addition to a weak bump $2\theta \sim 44$ degrees.

To obtain more information on the surface changes of PGP-Mn1 after 24 and 72 h of immersion in both media, SEM imaging was performed (Figure 11). Before immersion, the surface of the glass particles appears smooth (as in Figure SI-1). After immersion in CM for 24 h, the formation of clusters of microspheres, with an average diameter of $3\text{--}4\text{ }\mu\text{m}$ (Figure 11A). Their number increases after 72 h of immersion, but their size remains unchanged (Figure 11B).

After immersion in Tris-B, flake-like microstructures ($6\text{--}9\text{ }\mu\text{m}$ in size) can be seen after 24 and 72 h of immersion (Figure 11C and D, respectively).





View Article Online
DOI: 10.1039/D5TB00454C

Figure 11. SEM micrographs of PGP-Mn1 after immersion in CM for 24 (A) and 72 h (B) and after immersion in Tris-B for 24 h (C) and 72 h (D).

4. Discussion

Rheology measurements of polyphosphate gels show that an increase in Mn^{2+} content leads to a rise in viscosity. This could be explained by two mechanisms: Mn^{2+} could screen the electrostatic repulsion between negatively charged phosphate chains, allowing them to get closer and therefore favouring their hydrophobic interactions, and/or act as an ionic cross-linker, causing intermolecular bridging between polyphosphate chains, therefore leading to an increase of the network strength.³¹ The increase in viscosity with Mn^{2+} content made the ES process more challenging; this could explain the presence of an increased number of fragmented fibres with increasing Mn^{2+} content.



Both PGPs and PGFs were manufactured starting from the same coacervate gel, via vacuum drying and ES, respectively. As demonstrated by XRPD analysis, the incorporation of Mn^{2+} , even up to 10 mol %, in both PGPs and PGFs does not induce crystallization. This finding is consistent with previous works on Mn loaded fluorophosphate-based glasses synthesized via MQ,¹⁸ with coacervate-made PGs loaded with various TMIs, such as Ag^+ and Fe^{3+} (up to 10 mol %),⁹ Ga^{3+} (up to 1 mol %),¹⁴ Zn^{2+} and Cu^{2+} (up to 15 mol %)^{13,42} and with SG-made PGs loaded with Sr^{2+} , Cu^{2+} and Zn^{2+} (up to 5 mol%).^{43–45} A summary of the key findings of these works is presented in Table SI-2.

Even though Mn^{2+} has been demonstrated to affect the viscosity of the gel, spectroscopic studies (FT-IR and Raman) indicate that the addition of Mn^{2+} does not significantly affect the structure of the phosphate network. This is in agreement with previous results on coacervate- and SG-made PGs, whose structure is not significantly affected by TMI addition.^{9,13,14,33,43} FT-IR and Raman spectra of PGPs and PGFs are very similar, the only difference being the absence of the in-chain $\text{Q}^2 \text{P}-\text{O}-\text{P}$ asymmetric stretching mode at $\sim 900 \text{ cm}^{-1}$ in the Raman spectrum of PGFs, which is instead present in the spectrum of PGPs.

PGPs and PGFs show comparable release profiles for all elements. For both PGPs and PGFs, there is a clear relationship between P, Na and Mn release and Mn loading. In particular, with increasing Mn loading there is an increase in the release of P and Mn, whereas the release of Na decreases. Such clear trend is not observed for Ca release. An increase of P release with increasing Mn loading could be explained with the weakening of the network by addition of Mn^{2+} .

There are conflicting reports in the literature regarding the role of Mn^{2+} on durability of glasses. Some reports that the incorporation of Mn on 45S5 glass (46.1 SiO_2 - 24.4 Na_2O - 26.9 CaO - 2.6 P_2O_5 mol %, $0.5 \leq \text{MnO} \leq 4$ mol %) increases the glass durability, probably due to the replacement of Ca-O bonds with the stronger Mn-O bonds.⁴⁶



However, other studies report an increase in solubility with increasing Mn loading of PGs prepared via MQ,⁴⁷ caused by gradual depolymerization of the phosphate network.

As our spectroscopic analysis does not indicate major differences in the structure of the network with Mn loading, a more advanced, synchrotron based atomic-scale analysis of the position of Mn²⁺ within the phosphate chain would be necessary to fully understand the observed trends.

The effect of dissolution products on the viability of MG-63 cells revealed viabilities above 72 % for PGPs-MnX and above 81 % for PGFs-MnX. These findings are consistent with previous reports on silicate-based glass nanoparticles doped with Mn²⁺ which demonstrated good cytocompatibility.⁴⁸ PGPs loaded with copper ions prepared via coacervation, have also shown MG-63 cell viability slightly higher than the control group at for copper loading up to 10 mol %, while higher copper content led to a decrease in viability, still considered in the non-toxic regime (~ 79 %).⁴² Similarly, Zn²⁺ loaded PGPs made via coacervation (up to 15 mol %) showed MG-63 cell viability values comparable to the control, with no cytotoxic effects observed even at the highest Zn²⁺ concentrations.⁴²

In this work, the highest cell viabilities % were observed for dissolution products deriving from PGPs and PGFs containing 1 mol % of Mn²⁺. Therefore, preliminary bioactivity evaluation was done on the selected sample PGP-Mn1. This choice was also supported by previous studies on Mn loaded 45S5-silicate glasses, where a MnO concentrations up to 1 mol % promoted apatite formation within 7 days upon immersion in SBF, whereas higher MnO contents (≥ 2 mol %) delayed or inhibited HA deposition.⁴⁶

Results revealed surface changes upon immersion in both Tris-B and CM. In particular, the attenuation of the FT-IR band associated with the asymmetric stretching of Q² phosphate units,



together with the emergence of new bands and shoulders attributed to phosphate groups typically found in HA nanoparticles, suggest the onset of HA-like phase formation.^{41,49–51} These findings are further supported by XRPD patterns, which display weak and broad peaks overlapping the amorphous halo, indicative of a nano-disordered phase. SEM analysis corroborates the spectroscopic and structural results, revealing distinct surface morphologies depending on the medium: spherical aggregates in CM and flake-like deposits in Tris-B. Similar spherical features were previously observed by Li *et al.*²⁷ after immersion of mesoporous PGs in SBF for 21 days.

The highly disordered nature of the phase formed on the surface of PGP-Mn1 following immersion in both CM and Tris-B is as suggested by structural, spectroscopic and surface analysis make its identification very challenging. Such challenge has also been faced in previous work of SG-derived mesoporous PGs, where phases formed after even longer immersion time in SBF were reported of difficult identification.²⁷ Nevertheless, the results presented here are very promising, as surface changes can be observed in a quite short immersion time compared to previous reports, indicating a possible higher bioactivity of the coacervate made PGs.

Conclusions

This work has demonstrated the versatility of the sustainable manufacturing technique of coacervation, which allows the production of PGs in the system P_2O_5 -CaO- Na_2O -MnO ($Mn^{2+} = 1, 3, 5, 10$ mol %) in both powder bulk and fibrous form. XRPD patterns of all PGs show that the presence of Mn^{2+} up to 10 mol % does not induce crystallisation.

The structure of the phosphate network in both PGPs and PGFs is similar, as demonstrated by FT-IR analysis. The structure is also similar to that of PGs prepared via MQ and SG, which confirms the success of the novel manufacturing technique of coacervation in producing similar PGs in a more sustainable and cost-effective way.



PGPs and PGFs dissolution studies showed that the release of P increases with Mn^{2+} loading, suggesting a weakness of the network upon Mn^{2+} addition.

Dissolution products from PGPs and PFGs in DI water show good cytocompatibility on osteosarcoma MG-63 cells with cell viability higher than ~72 % for PGPs and higher than ~ 81 % for PGFs.

Preliminary bioactivity testing carried out on a representative powder sample, PGP-Mn1, indicate the formation of a disordered phase, most likely an HA-like phase, following 24 and 72 h of immersion in CM and Tris-B.

Supporting Information: compositions of PGPs and PGFs expressed in atomic % measured via EDX; summary of key references on PGs; SEM image of PGP-Mn1; FT-IR spectra of PGP-Mn1 before (a) and after immersion in CM for 24 h (b), 72 h (c) and after immersion in Tris-B for 24 h (d), 72 h (e).

Conflict of interest: there are no conflicts to declare.

Data availability: the data supporting this article have been included as part of the Supplementary Information.

Acknowledgments

The authors are also grateful to Dr David Jones for his help with the SEM/EDX, Dr Rachida-Bounce for assistance with IR/Raman spectroscopies and Dr Driscoll (University of Surrey) for his help with the XRPD.

Funding sources



The authors would like to acknowledge EPSRC (grant EP/P033636/1), Royal Society (grant RSG\R1\180191) and Royal Society of Chemistry Fund Grant (R21-7668912428 and R24-9885329913) for providing the funding to conduct this study. The authors thank the EPSRC for providing the capital funding that funded the Raman microscope used in this work (EP/M022749/1). Thanks to the Doctoral College, University of Surrey for funding Z. Moghaddam PhD studentship and the University of Surrey and ICase NPL for funding R. Di Pasquale's PhD studentship. Chiara Cavazzoli acknowledges the University of Modena, Department of Chemical and Geological Sciences, for providing Extra -EU Fellowship (Dept. Prot. Prot. 0115375) to conduct this study.

References

- (1) Vemula, P. K.; Cruikshank, G. A.; Karp, J. M.; John, G. Self-Assembled Prodrugs: An Enzymatically Triggered Drug-Delivery Platform. *Biomaterials* **2009**, *30* (3), 383–393. <https://doi.org/10.1016/j.biomaterials.2008.09.045>.
- (2) Kaur, G.; Pickrell, G.; Sriranganathan, N.; Kumar, V.; Homa, D. Review and the State of the Art: Sol-Gel and Melt Quenched Bioactive Glasses for Tissue Engineering. *J Biomed Mater Res B Appl Biomater* **2016**, *104* 6, 1248–1275.
- (3) Kyffin, B. A.; Foroutan, F.; Raja, F. N. S.; Martin, R. A.; Pickup, D. M.; Taylor, S. E.; Carta, D. Antibacterial Silver-Doped Phosphate-Based Glasses Prepared by Coacervation. *J. Mater. Chem. B* **2019**, *7* (48), 7744–7755. <https://doi.org/10.1039/C9TB02195G>.
- (4) Mouriño, V.; Cattalini, J.; Boccaccini, A. Metallic Ions as Therapeutic Agents in Tissue Engineering Scaffolds: An Overview of Their Biological Applications and Strategies for New Developments. *Journal of the Royal Society, Interface / the Royal Society* **2011**, *9*, 401–419. <https://doi.org/10.1098/rsif.2011.0611>.



- (5) Abou Neel, E. A.; Pickup, D. M.; Valappil, S. P.; Newport, R. J.; Knowles, J. C. Bioactive Functional Materials: A Perspective on Phosphate-Based Glasses. *J. Mater. Chem.* **2009**, *19* (6), 690–701. <https://doi.org/10.1039/B810675D>. View Article Online
DOI: 10.1039/D51B00454C
- (6) Lapa, A.; Cresswell, M.; Jackson, P.; Boccaccini, A. Phosphate Glass Fibres with Therapeutic Ions Release Capability – a Review. *Advances in Applied Ceramics* **2019**, *119*. <https://doi.org/10.1080/17436753.2018.1564413>.
- (7) Ahmed, I.; Lewis, M.; Olsen, I.; Knowles, J. C. Phosphate Glasses for Tissue Engineering: Part 1. Processing and Characterisation of a Ternary-Based P₂O₅–CaO–Na₂O Glass System. *Biomaterials* **2004**, *25* (3), 491–499. [https://doi.org/https://doi.org/10.1016/S0142-9612\(03\)00546-5](https://doi.org/10.1016/S0142-9612(03)00546-5).
- (8) Łapa, A.; Cresswell, M.; Campbell, I.; Jackson, P.; Goldmann, W. H.; Detsch, R.; Parsons, A.; Ahmed, I.; Boccaccini, A. R. Ga and Ce Ion-Doped Phosphate Glass Fibres with Antibacterial Properties and Their Composite for Wound Healing Applications. *J. Mater. Chem. B* **2019**, *7* (44), 6981–6993. <https://doi.org/10.1039/C9TB00820A>.
- (9) Hoxha, A.; Nikolaou, A.; Wilkinson, H. N.; Hardman, M. J.; Gutierrez-Merino, J.; Felipe-Sotelo, M.; Carta, D. Wound Healing Promotion via Release of Therapeutic Metallic Ions from Phosphate Glass Fibers: An In Vitro and Ex Vivo Study. *ACS Appl Mater Interfaces* **2024**, *16* (29), 37669–37682. <https://doi.org/10.1021/acsami.4c07035>.
- (10) Carta, D.; Pickup, D. M.; Foroutan, F. Phosphate-Based Glasses Prepared via Sol–Gel and Coacervation. In *Phosphate and Borate Bioactive Glasses*; Obata, A., Brauer, D. S., Kasuga, T., Eds.; The Royal Society of Chemistry, 2022; p 0. <https://doi.org/10.1039/9781839164750-00078>.



- (11) Pickup, D.; Newport, R.; Barney, E.; Kim, J.-Y.; Valappil, S.; Knowles, J. Characterisation of Phosphate Coacervates for Potential Biomedical Applications. *J Biomater Appl* **2013**, *28*. <https://doi.org/10.1177/0885328213502586>. View Article Online
DOI: 10.1039/D5TB00454C
- (12) Kyffin, B. A.; Di Pasquale, R.; Pickup, D. M.; Foroutan, F.; Abrahams, I.; Kanwal, N.; Keeble, D. S.; Felipe-Sotelo, M.; Hoxha, A.; Moghaddam, Z.; Hinder, S. J.; Baker, M. A.; Nery, E. T.; Carta, D. Atomic Scale Investigation and Cytocompatibility of Copper and Zinc-Loaded Phosphate-Based Glasses Prepared by Coacervation. *Materialia (Oxf)* **2024**, *38*, 102246. <https://doi.org/https://doi.org/10.1016/j.mtla.2024.102246>.
- (13) Foroutan, F.; Nikolaou, A.; Kyffin, B. A.; Elliott, R. M.; Felipe-Sotelo, M.; Gutierrez-Merino, J.; Carta, D. Multifunctional Phosphate-Based Glass Fibres Prepared via Electrospinning of Coacervate Precursors: Controlled Delivery, Biocompatibility and Antibacterial Activity. *Materialia (Oxf)* **2020**, *14*, 100939. <https://doi.org/10.1016/j.mtla.2020.100939>.
- (14) Moghaddam, Z.; Nery, E. T.; Unalan, I.; Hoxha, A.; Felipe-Sotelo, M.; Zhao, H.; Pinna, A.; Abrahams, I.; Smales, G. J.; Boccaccini, A. R.; Carta, D. Electrospun Porous Phosphate-Based Glass Fibres Containing Gallium and Clove Oil: Cytotoxicity and Antioxidant Properties. *Ceram Int* **2025**. <https://doi.org/https://doi.org/10.1016/j.ceramint.2025.03.017>.
- (15) Srivastava, A.; Pyare, R.; Singh, S. I>In Vitro Bioactivity and Physical–Mechanical Properties of MnO₂ Substituted 45S5 Bioactive Glasses and Glass-Ceramics. *J Biomater Tissue Eng* **2012**, *2*, 249–258. <https://doi.org/10.1166/jbt.2012.1043>.
- (16) Sopyan, I.; Singh, R.; Nawawi, N.; Tampieri, A.; Sprio, S. Effects of Manganese Doping on Properties of Sol–Gel Derived Biphasic Calcium Phosphate Ceramics. *Ceram Int* **2011**, *37*, 3703–3715.



- (17) Fujitani, W.; Hamada, Y.; Kawaguchi, N.; Mori, S.; Daito, K.; Uchinaka, A.; Matsumoto, T.; Kojima, Y.; Daito, M.; Nakano, T.; Matsuura, N. Synthesis of Hydroxyapatite Containing Manganese and Its Evaluation of Biocompatibility. *Nano Biomedicine* **2010**, *2*, 37–46. DOI: 10.1039/D5TB00454C
- (18) Chand, N. R. K.; Sudhakar, B. K.; Guntu, R. K.; Rao, G.; Rao, C. Influence of Manganese Ions on Elastic and Spectroscopic Properties of ZnO Doped Novel Calcium Fluorophosphate Bio Active Glasses. *Phys Scr* **2021**, *96*. <https://doi.org/10.1088/1402-4896/ac2d7c>.
- (19) Islam, M. T.; Felfel, R. M.; Abou Neel, E. A.; Grant, D. M.; Ahmed, I.; Hossain, K. M. Z. Bioactive Calcium Phosphate-Based Glasses and Ceramics and Their Biomedical Applications: A Review. *J Tissue Eng* **2017**, *8*, 204173141771917. <https://doi.org/10.1177/2041731417719170>.
- (20) Popa, A. C.; Stan, G.; Husanu, M.-A.; Mercioniu, I.; Santos, L.; Fernandes, H.; Ferreira, J. Bioglass Implant-Coating Interactions in Synthetic Physiological Fluids with Varying Degrees of Biomimicry. *Int J Nanomedicine* **2017**, *Volume 12*, 683–707. <https://doi.org/10.2147/IJN.S123236>.
- (21) Wetzel, R.; Brauer, D. Apatite Formation of Substituted Bioglass 45S5: SBF vs. Tris. *Mater Lett* **2019**, *257*, 126760. <https://doi.org/10.1016/j.matlet.2019.126760>.
- (22) Kokubo, T.; Takadama, H. How Useful Is SBF in Predicting in Vivo Bone Bioactivity? *Biomaterials* **2006**, *27*, 2907–2915. <https://doi.org/10.1016/j.biomaterials.2006.01.017>.
- (23) *Phosphate and Borate Bioactive Glasses*; Obata, A., Brauer, D. S., Kasuga, T., Eds.; The Royal Society of Chemistry, 2022. <https://doi.org/10.1039/9781839164750>.



- (24) Babu, M. M.; Rao, P. V.; Singh, R. K.; Kim, H.-W.; Veeraiah, N.; Özcan, M.; Prasad, P. S. ZnO Incorporated High Phosphate Bioactive Glasses for Guided Bone Regeneration Implants: Enhancement of in Vitro Bioactivity and Antibacterial Activity. *Journal of Materials Research and Technology* **2021**, *15*, 633–646. <https://doi.org/10.1016/j.jmrt.2021.08.020>. DOI: 10.1039/D5TB00454C
- (25) OHTSUKI, C.; KOKUBO, T.; TAKATSUKA, K.; YAMAMURO, T. Compositional Dependence of Bioactivity of Glasses in the System CaO-SiO₂-P₂O₅. *Journal of the Ceramic Society of Japan* **1991**, *99* (1145), 1–6. <https://doi.org/10.2109/jcersj.99.1>.
- (26) KASUGA, T.; HOSOI, Y.; NOGAMI, M.; NIINOMI, M. BIOMIMETIC APATITE FORMATION ON CALCIUM PHOSPHATE INVERT GLASSES. *Phosphorus Research Bulletin* **2001**, *12*, 39–44. https://doi.org/10.3363/prb1992.12.0_39.
- (27) Li, C.; Wang, C.; Boccaccini, A. R.; Zheng, K. Sol-Gel Processing and Characterization of Binary P₂O₅-CaO and Ternary P₂O₅-CaO-Li₂O Mesoporous Phosphate Bioactive Glasses. *Journal of Non-Crystalline Solids: X* **2023**, *17*, 100159. <https://doi.org/10.1016/j.nocx.2023.100159>.
- (28) Kaou, M. H.; Furkó, M.; Balázs, K.; Balázs, C. Advanced Bioactive Glasses: The Newest Achievements and Breakthroughs in the Area. *Nanomaterials* **2023**, *13* (16). <https://doi.org/10.3390/nano13162287>.
- (29) Kumar, G. A.; Rambabu, Y.; Guntu, R. K.; Sivaram, K.; Reddy, M. S.; Rao, Ch. S.; Venkatramu, V.; Kumar, V. R.; Sriraman Narayana Iyengar, N. Ch. ZrxCa30-XP70 Thermoluminescent Bio Glass, Structure and Elasticity. *J Mech Behav Biomed Mater* **2021**, *119*, 104517. <https://doi.org/10.1016/j.jmbbm.2021.104517>.



- (30) Nommeots-Nomm, A.; Hupa, L.; Rohanova, D.; Brauer, D. A Review of Acellular Immersion Tests on Bioactive Glasses—Influence of Medium on Ion Release and Apatite Formation. *Int J Appl Glass Sci* **2020**, *11*. <https://doi.org/10.1111/ijag.15006>. View Article Online
DOI: 10.1039/D5TB00454C
- (31) Momeni, A.; Filiaggi, M. J. Rheology of Polyphosphate Coacervates. *J Rheol (N Y N Y)* **2016**, *60* (1), 25–34. <https://doi.org/10.1122/1.4935127>.
- (32) Nikolaou, A.; Felipe-Sotelo, M.; Dorey, R.; Gutierrez-Merino, J.; Carta, D. Silver-Doped Phosphate Coacervates to Inhibit Pathogenic Bacteria Associated with Wound Infections: An in Vitro Study. *Sci Rep* **2022**, *12* (1), 10778. <https://doi.org/10.1038/s41598-022-13375-y>.
- (33) Humphray, J.; Hoxha, A.; Tomás Nery, E.; Berry, C.; Felipe-Sotelo, M.; Wilkinson, H.; Hardman, M.; Gutiérrez-Merino, J.; Carta, D. Electrospun Polyphosphate Coacervate Glass Fibers in the System P₂O₅–CaO–MgO–Na₂O–Fe₂O₃ for Wound Healing. *ACS Omega* **2025**, *10* (11), 10987–10996. <https://doi.org/10.1021/acsomega.4c09366>.
- (34) AlQaysi, M.; Walters, N.; Foroutan, F.; Owens, G.; Kim, H.-W.; Shah, R.; Knowles, J. Strontium- and Calcium-Containing, Titanium-Stabilised Phosphate-Based Glasses with Prolonged Degradation for Orthopaedic Tissue Engineering. *J Biomater Appl* **2015**, *30*, 300–310.
- (35) Carta, D.; Pickup, D. M.; Knowles, J. C.; Smith, M. E.; Newport, R. J. Sol–Gel Synthesis of the P₂O₅–CaO–Na₂O–SiO₂ System as a Novel Bioresorbable Glass. *J. Mater. Chem.* **2005**, *15* (21), 2134–2140. <https://doi.org/10.1039/B414885A>.
- (36) Abou Neel, E.; Salih, V.; Knowles, J. 1.18 Phosphate-Based Glasses. In *Comprehensive Biomaterials*; 2017; pp 392–405. <https://doi.org/10.1016/B978-0-08-100691-7.00253-6>.



- (37) Foroutan, F.; Walters, N.; Owens, G.; Mordan, N.; Kim, H.-W.; Leeuw, N.; Knowles, J. Sol-Gel Synthesis of Quaternary $(\text{P}_2\text{O}_5)_{55}-(\text{CaO})_{25}-(\text{Na}_2\text{O})_{(20-X)}-(\text{TiO}_2)_X$ Bioresorbable Glasses for Bone Tissue Engineering Applications ($X = 0, 5, 10, \text{ or } 15$). *Biomedical Materials* **2015**, *10*. <https://doi.org/10.1088/1748-6041/10/4/045025>. View Article Online
DOI: 10.1039/D5TB00454C
- (38) Foroutan, F.; Jokerst, J. V.; Gambhir, S. S.; Vermesh, O.; Kim, H.-W.; Knowles, J. C. Sol-Gel Synthesis and Electrospraying of Biodegradable $(\text{P}_2\text{O}_5)_{55}-(\text{CaO})_{30}-(\text{Na}_2\text{O})_{15}$ Glass Nanospheres as a Transient Contrast Agent for Ultrasound Stem Cell Imaging. *ACS Nano* **2015**, *9* (2), 1868–1877. <https://doi.org/10.1021/nn506789y>.
- (39) Muñoz Francisco and Rocherullé, J. and A. I. and H. L. Phosphate Glasses. In *Springer Handbook of Glass*; Musgraves J. David and Hu, J. and C. L., Ed.; Springer International Publishing: Cham, 2019; pp 553–594. https://doi.org/10.1007/978-3-319-93728-1_16.
- (40) Baia, L.; Muresan, D.; Baia, M.; Popp, J.; Simon, S. Structural Properties of Silver Nanoclusters–Phosphate Glass Composites. *Vib Spectrosc* **2007**, *43* (2), 313–318. <https://doi.org/https://doi.org/10.1016/j.vibspec.2006.03.006>.
- (41) Foroutan, F.; Kyffin, B. A.; Abrahams, I.; Corrias, A.; Gupta, P.; Velliou, E.; Knowles, J. C.; Carta, D. Mesoporous Phosphate-Based Glasses Prepared via Sol–Gel. *ACS Biomater Sci Eng* **2020**, *6* (3), 1428–1437. <https://doi.org/10.1021/acsbiomaterials.9b01896>.
- (42) Kyffin, B. A.; Di Pasquale, R.; Pickup, D. M.; Foroutan, F.; Abrahams, I.; Kanwal, N.; Keeble, D. S.; Felipe-Sotelo, M.; Hoxha, A.; Moghaddam, Z.; Hinder, S. J.; Baker, M. A.; Nery, E. T.; Carta, D. Atomic Scale Investigation and Cytocompatibility of Copper and Zinc-Loaded Phosphate-Based Glasses Prepared by Coacervation. *Materialia (Oxf)* **2024**, *38*, 102246. <https://doi.org/https://doi.org/10.1016/j.mtla.2024.102246>.



- (43) Foroutan, F.; Kyffin, B.; Abrahams, I.; Knowles, J.; Sogne, E.; Falqui, A.; Carta, D. Mesoporous Strontium-Doped Phosphate-Based Sol-Gel Glasses for Biomedical Applications. *Front Chem* **2020**, *8*, 249. <https://doi.org/10.3389/fchem.2020.00249>. View Article Online
DOI: 10.1039/D3TB00454C
- (44) Foroutan, F.; Kyffin, B. A.; Nikolaou, A.; Merino-Gutierrez, J.; Abrahams, I.; Kanwal, N.; Knowles, J. C.; Smith, A. J.; Smales, G. J.; Carta, D. Highly Porous Phosphate-Based Glasses for Controlled Delivery of Antibacterial Cu Ions Prepared via Sol–Gel Chemistry. *RSC Adv.* **2023**, *13* (29), 19662–19673. <https://doi.org/10.1039/D3RA02958A>.
- (45) Foroutan, F.; Abrahams, I.; Smales, G. J.; Kanwal, N.; di Pasquale, R.; Knowles, J. C.; Smith, A. J.; Carta, D. A Sol-Gel Templating Route for the Synthesis of Hierarchical Porous Calcium Phosphate Glasses Containing Zinc. *Ceram Int* **2024**, *50* (20, Part A), 38174–38182. <https://doi.org/https://doi.org/10.1016/j.ceramint.2024.07.180>.
- (46) Abati, M.; Contreras Jaimes, A. T.; Rigamonti, L.; Carrozza, D.; Lusvardi, G.; Brauer, D. S.; Malavasi, G. Assessing Mn as an Antioxidant Agent in Bioactive Glasses by Quantification of Catalase and Superoxide Dismutase Enzymatic Mimetic Activities. *Ceram Int* **2024**, *50* (2, Part A), 2574–2587. <https://doi.org/https://doi.org/10.1016/j.ceramint.2023.10.091>.
- (47) Szumera, M. The Structural Role of Manganese Ions in Soil Active Silicate–Phosphate Glasses. *Spectrochim Acta A Mol Biomol Spectrosc* **2014**, *129*, 601–608. <https://doi.org/https://doi.org/10.1016/j.saa.2014.03.102>.
- (48) Westhauser, F.; Wilkesmann, S.; Nawaz, Q.; Schmitz, S. I.; Moghaddam, A.; Boccaccini, A. R. Osteogenic Properties of Manganese-Doped Mesoporous Bioactive Glass Nanoparticles. *J Biomed Mater Res A* **2020**, *108* (9), 1806–1815. <https://doi.org/https://doi.org/10.1002/jbm.a.36945>.



- (49) Coelho, C. C.; Grenho, L.; Gomes, P. S.; Quadros, P. A.; Fernandes, M. H. Nano-Hydroxyapatite in Oral Care Cosmetics: Characterization and Cytotoxicity Assessment. *Sci Rep* **2019**, 9 (1), 11050. <https://doi.org/10.1038/s41598-019-47491-z>. View Article Online
DOI: 10.1039/D5TB00454C
- (50) Kourkouvelis, N.; Tzaphlidou, M. Spectroscopic Assessment of Normal Cortical Bone: Differences in Relation to Bone Site and Sex. *ScientificWorldJournal* **2010**, 10, 402–412. <https://doi.org/10.1100/tsw.2010.43>.
- (51) Mooney, R. W.; Toma, S. Z.; Goldsmith, R. L.; Butler, K. H. Normal Vibrations of the PO₄³⁻ Ion, Site Symmetry C_{3v}, IN Sr₃(PO₄)₂ and Ba₃(PO₄)₂. *Journal of Inorganic and Nuclear Chemistry* **1968**, 30 (7), 1669–1675. [https://doi.org/https://doi.org/10.1016/0022-1902\(68\)80337-9](https://doi.org/10.1016/0022-1902(68)80337-9).



The data supporting this article have been included as part of the Supplementary Information.

